environmental microbiology

Environmental Microbiology (2012) doi:10.1111/j.1462-2920.2012.02825.x

# Anaerobic methane oxidation in metalliferous hydrothermal sediments: influence on carbon flux and decoupling from sulfate reduction

**Scott D. Wankel,[1,2†] Melissa M. Adams,[1†] David T. Johnston,[2] Colleen M. Hansel,[3] Samantha B. Joye[4] and Peter R. Girguis[1*]**

[1]*Department of Organismic and Evolutionary Biology,* [2]*Department of Earth and Planetary Sciences, Harvard University,* [3]*School of Engineering and Applied Science, Harvard University, Cambridge, MA 01238, USA.* [4]*Department of Marine Sciences, University of Georgia, Athens, GA 30602-3636, USA.*

## Summary

**The anaerobic oxidation of methane (AOM) is a globally significant sink that regulates methane flux from sediments into the oceans and atmosphere. Here we examine mesophilic to thermophilic AOM in hydrothermal sediments recovered from the Middle Valley vent field, on the Juan de Fuca Ridge. Using continuous-flow sediment bioreactors and batch incubations, we characterized (i) the degree to which AOM contributes to net dissolved inorganic carbon flux, (ii) AOM and sulfate reduction (SR) rates as a function of temperature and (iii) the distribution and density of known anaerobic methanotrophs (ANMEs). In sediment bioreactors, inorganic carbon stable isotope mass balances results indicated that AOM accounted for between 16% and 86% of the inorganic carbon produced, underscoring the role of AOM in governing inorganic carbon flux from these sediments. At 90°C, AOM occurred in the absence of SR, demonstrating a striking decoupling of AOM from SR. An abundance of Fe(III)-bearing minerals resembling mixed valent Fe oxides, such as green rust, suggests the potential for a coupling of AOM to Fe(III) reduction in these metalliferous sediments. While SR bacteria were only observed in cooler temperature sediments, ANMEs allied to ANME-1 ribotypes, including a putative ANME-1c group, were found across all temperature regimes and represented a substantial proportion of the archaeal community. In concert, these results extend and reshape our understanding of the nature of high temperature methane biogeochemistry, providing insight into the physiology and ecology of thermophilic anaerobic methanotrophy and suggesting that AOM may play a central role in regulating biological dissolved inorganic carbon fluxes to the deep ocean from the organic-poor, metalliferous sediments of the global mid-ocean ridge hydrothermal vent system.**

Received 11 November, 2011; revised 3 May, 2012; accepted 17 June, 2012. *For correspondence. E-mail pgirguis@oeb.harvard.edu; Tel. (+1) 617 496 8328; Fax (+1) 617 495 8848. †Authors contributed equally.

## Introduction

Methane, a potent greenhouse gas, is biologically cycled in a diversity of ecosystems ranging from terrestrial soils to high-arctic lakes to hydrothermal vents and hydrocarbon seeps (Walter *et al.*, 2006; Reeburgh, 2007; Valentine, 2011). In marine sediments, investigations of microbially mediated methane cycling have largely focused on characterizing the anaerobic oxidation of methane (AOM) (for reviews, see Conrad, 2009; Knittel and Boetius, 2009; Valentine, 2011), as AOM is estimated to consume ~75% of the methane produced in marine sediments (Reeburgh, 2007). Geochemical studies (Martens and Berner, 1974; Reeburgh, 1976; Alperin *et al.*, 1988; Hoehler *et al.*, 1994; Lapham *et al.*, 2008a), radiotracer metabolic assessments (Alperin and Reeburgh, 1985; Iversen and Jorgensen, 1985; Joye *et al.*, 2004), laboratory incubations (Alperin and Reeburgh, 1985; Nauhaus *et al.*, 2002; 2007; Girguis *et al.*, 2003; 2005) and molecular microbiological studies (Hinrichs *et al.*, 1999; Boetius *et al.*, 2000; Orphan *et al.*, 2001; 2002; Biddle *et al.*, 2011; Lloyd *et al.*, 2011) have demonstrated a coupling and close spatial association of anaerobic methanotrophs (ANMEs) and sulfate reducers (SRB). The syntrophic interaction of these groups is thought to mediate AOM, although stoichiometric variations in the coupling between AOM and sulfate reduction (SR) have also been observed, likely as a function of organic matter availability (Kallmeyer and Boetius, 2004; Nauhaus *et al.*, 2005; Orcutt *et al.*, 2005; Meulepas *et al.*, 2009; Bowles *et al.*, 2011; Burdige and Komada, 2011). AOM has also been linked to reduction of other electron acceptors,

including oxidized species of N, Fe and Mn, although previously observed rates were modest (Ragshoebarsing *et al.*, 2006; Beal *et al.*, 2009; Ettwig *et al.*, 2010).

Although the majority of work to date has targeted low-temperature marine ecosystems, research has begun to shed light on the role of AOM in higher temperature environments. Recent studies of AOM in Guaymas Basin, a sedimented and organic-rich hydrothermal field, have shown that AOM and SR can occur across a range of elevated temperatures, and that the coupling of AOM and SR continues at elevated temperatures (Schouten *et al.*, 2003; Kallmeyer and Boetius, 2004; Biddle *et al.*, 2011; Holler *et al.*, 2011). Given the ubiquity of hydrothermal systems along the mid-ocean ridge system, and their important role in biogeochemical cycles (Wheat *et al.*, 2003; Coumou *et al.*, 2008; Tagliabue *et al.*, 2010) determining the significance of AOM in these systems is a major step towards improving constraints on methane dynamics at a global scale. Of particular interest is the importance of AOM and SR in hydrothermal environments characterized by high-temperature sediments and fluids that are high in methane, metal-rich (or metalliferous), but contain lower amounts of organic carbon. Such metalliferous environments might further foster the coupling of AOM to others oxidants such as metal oxides, especially when the organic carbon load, and associated sulfate reduction rates, are low.

The Middle Valley hydrothermal vent field – an extensional axial rift valley located on the northern end of the Juan de Fuca Ridge – is an appropriate environment for investigating the nature and extent of AOM at elevated temperatures and lower organic carbon. In contrast to Guaymas Basin, a relatively well-studied hydrothermal vent system hosting very organic-rich sediments, Middle Valley represents a system that is more typical of mid-ocean ridge hydrothermal vents worldwide. The vent fluids and metal rich sediments of Middle Valley contain high concentrations of reduced compounds, such as $H_2$, $H_2S$ and $CH_4$ (Ames *et al.*, 1993; Rushdl and Simonelt, 2002; Cruse and Seewald, 2006; 2010; Cruse *et al.*, 2008), and metals such as Fe, Cr and As, as well as the presence of oxidized Fe minerals including lepidocrocite (Goodfellow and Blaise, 1988; Ames *et al.*, 1993).

Here we present an integrative biogeochemical investigation of mesophilic and thermophilic AOM in metalliferous hydrothermal sediments that examines (i) the contribution of AOM to net inorganic carbon production, (ii) net AOM and SR rates as a function of temperature, (iii) the coupling of AOM and SR across temperatures and (iv) the diversity, phylogeny and distribution of the microbial community catalysing AOM in these hydrothermal sediments. Using thermal gradient, continuous-flow bioreactors (Fig. 1), the contribution of AOM to carbon cycling, as well as net AOM rates, were constrained via carbon stable isotope mass balance. The coupling of AOM and SR as a function of temperature was addressed by using sediment slurry incubations (herein referred to as 'batch' incubations) that enable the measurement and comparison of AOM and SR rate measurements in a closed system and at discrete, environmentally relevant temperatures (20°C, 55°C and 90°C). Archaeal and bacterial diversity in the whole sediment core incubations was characterized via massively paralleled pyrosequencing, and known ANMEs were quantified using quantitative PCR and visualized via fluorescent *in situ* hybridization (FISH). Collectively, these data provide insight into AOM

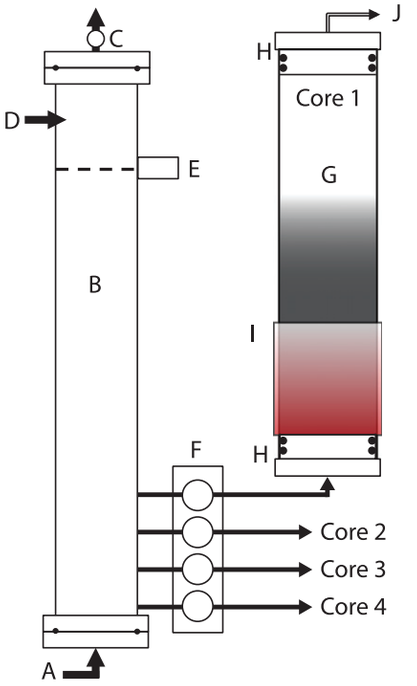


**Fig. 1.** Schematic of the high temperature, continuous flow bioreactor with only one sediment core shown (for simplicity). To reproduce hydrothermal vent-like influent for percolation through the sediments, gas mixtures containing methane, hydrogen sulfide, and nitrogen were delivered (A) via mass flow controllers into the bottom of a 1 m long polyvinylchloride gas equilibration column (B). Headspace pressure in the column was maintained with a back pressure regulator (C) and fluid level was maintained by automatically addition of filter- and UV-sterilized seawater (D). Seawater level was controlled via a float-activated relay (E), allowing the solution to equilibrate with the headspace. Simulated vent fluid was delivered to each core using a multi-channel, peristaltic pump (F) with gastight vinyl tubing. 30 cm long polycarbonate columns (6.4 cm ID; 0.64 cm wall) (G) fit with custom double o-ring sealed top and bottom plugs (H) housed the sediment cores and enabled long-term irrigation. Thermostatically controlled heating jackets (I) were used to establish thermal gradients from ~ 90°C to 25°C. Fluid and gas samples were regularly collected from both the influent stream in the effluent stream from the top of each core (J) throughout incubation.

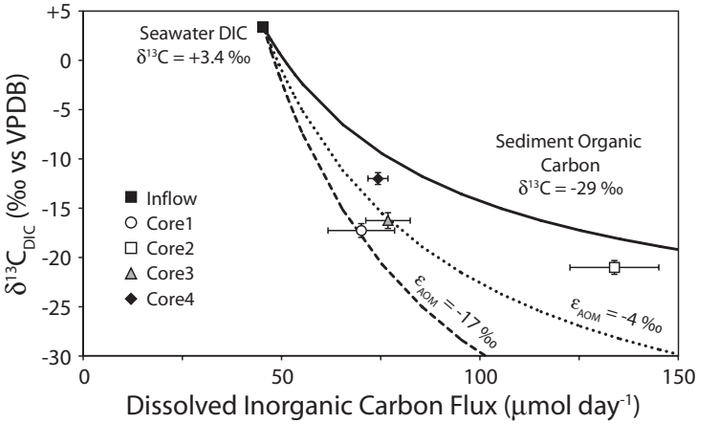


**Fig. 2.** Stable carbon isotope ($\delta^{13}C$) mixing model illustrating steady-state flux and $\delta^{13}C$ of inflow and outflow dissolved inorganic carbon (DIC; μmol $day^{-1}$) in the flow-through core incubations. Mixing lines illustrate addition of DIC to background seawater (black square) from anaerobic oxidation of sediment organic carbon (solid line; $\delta^{13}C = -29 \pm 0.4$‰, $n = 21$) or methane (dashed lines; inflow $\delta^{13}C_{CH4} = -40.2 \pm 0.9$‰ with estimates of fractionation by AOM ($\varepsilon_{AOM}$) ranging from 4‰ to 17‰ based on estimates from previous sedimentary studies). Elevated outflow DIC fluxes and lower $\delta^{13}C_{DIC}$ values from all cores (relative to background seawater) indicate varying production of DIC by both processes.

and SR dynamics in hydrothermal sediments, the diversity and distribution of known and new groups of ANMEs across thermal and chemical gradients, and the significance of AOM in hydrothermal sediment carbon cycling.

## Results

### *Isotope mass balance constraints on AOM and OC oxidation from continuous flow incubations*

Inflow dissolved inorganic carbon (DIC) concentrations of inlet seawater remained constant (2.1 ± 0.1 mM) for the entire duration of the experiment. However, steady-state outflow DIC concentrations markedly increased in all four cores (Fig. 2), ranging from 2.6 to 4.9 mM (Table 1). Net DIC fluxes at steady state (inflow minus outflow) ranged from 8.2 to 28.6 mmol $m^{-2}$ $day^{-1}$ (Table 2). The change in outflow DIC stable carbon isotope ratio ($\delta^{13}C_{DIC}$) diverged from the inflow $\delta^{13}C_{DIC}$ (+3.4‰) to compositions ranging from –12.0‰ to –21.0‰ (Fig. 2). In contrast to the DIC, methane ($CH_4$) concentrations decreased substantially between inflow (~ 2.8 ± 0.6 mM) and outflow (< 0.3 mM) among all cores, reflecting steady-state $CH_4$ consumption in sediments. Periodic outgassing of $CH_4$ (ebullition) was observed as the $CH_4$-saturated inflow fluid travelled across thermal regimes, which precluded the use of changes in $CH_4$ concentration to validate the mass balance model, but otherwise had no substantive impact (see *Discussion*). $CH_4$ $\delta^{13}C$ exhibited small changes between inflow (–40.2‰) and outflow (–40.6‰ to –38.2‰). Bulk sediment organic carbon content was 0.4% and exhibited a homogenous $\delta^{13}C$ composition ranging from –28.7‰ to –29.3‰ (Table S1). Using a steady-state isotope mass balance model, estimates of DIC production by AOM ranged from 2.2 to 10.1 mmol $m^{-2}$ $day^{-1}$. Estimates of DIC production by OC oxidation ranged from 1.2 to 23.9 mmol $m^{-2}$ $day^{-1}$ (Table 2). Mass balance calculations of volumetric AOM and OC oxidation from the DIC isotope mass balance ranged from 11.1–51.2 nmol $cc^{-1}$ $day^{-1}$ and 0.0 to 132.9 nmol $cc^{-1}$ $day^{-1}$ respectively (Table 2). Thus, AOM accounted for 86–100%, 16–32%, 58–100% and 23–44% of the DIC produced in Cores 1 through 4 respectively. Sensitivity of these modelled rate

**Table 1.** Steady-state concentrations and carbon stable isotopic composition ($\delta^{13}C$) of DIC and $CH_4$ in the influent and effluent of the flow-through sediment core reactors, and average carbon content and stable isotopic composition of the sediment organic carbon.

| | Dissolved inorganic carbon | | Dissolved methane | | Sediment organic carbon | | |
|---|---|---|---|---|---|---|---|
| | mM | $\delta^{13}C$ (‰) | μM | $\delta^{13}C$ (‰) | *n* | % | $\delta^{13}C$ (‰) |
| Inflow | 2.11 ± 0.07 | 3.4 ± 0.5 | 2849 ± 643.9 | –40.2 ± 0.9 | | | |
| Core 1 | 2.56 ± 0.30 | –17.3 ± 0.7 | 133 ± 16.6 | –40.6 ± 0.2 | 7 | 0.40 ± 0.03 | –29.3 ± 0.6 |
| Core 2 | 4.86 ± 0.40 | –21.0 ± 0.7 | 243 ± 22.6 | –38.2 ± 0.2 | 7 | 0.40 ± 0.01 | –28.7 ± 1.9 |
| Core 3 | 2.77 ± 0.20 | –16.3 ± 0.8 | 216 ± 36.7 | –38.7 ± 0.5 | 10 | 0.41 ± 0.05 | –29.0 ± 0.4 |
| Core 4 | 2.70 ± 0.09 | –12.0 ± 0.6 | 261 ± 34.1 | –39.7 ± 0.1 | 7 | 0.41 ± 0.03 | –28.9 ± 0.2 |

See text for analytical methods and precision.

**Table 2.** Calculated rates of anaerobic oxidation of methane (AOM) and sediment organic carbon (OC).

| Integrated rates (mmol $m^{-2}$ $day^{-1}$) | | | | | | |
|---|---|---|---|---|---|---|
| | A. Whole core DIC isotope mass balance | | | | | B. Interpolated batch data |
| | | AOM | | Organic matter oxidation ($OrgC_{ox}$) | | |
| Core | DIC production | $\varepsilon_{AOM} = 4$ | $\varepsilon_{AOM} = 17$ | $\varepsilon_{AOM} = 4$ | $\varepsilon_{AOM} = 17$ | AOM |
| 1 | 8.2 | – | 7.0 | – | 1.2 | 12.9 |
| 2 | 28.6 | 9.2 | 4.6 | 19.3 | 23.9 | 14.0 |
| 3 | 10.1 | – | 5.8 | – | 4.3 | 19.1 |
| 4 | 9.5 | 4.2 | 2.2 | 5.3 | 7.3 | 16.2 |
| Volumetric rates (nmol $cc^{-1}$ $day^{-1}$) | | | | | | |
| | C. Whole core DIC isotope mass balance | | | | | D. Interpolated batch data |
| | | AOM | | Organic matter oxidation ($Org_{Cox}$) | | |
| Core | DIC production | $\varepsilon_{AOM} = 4$ | $\varepsilon_{AOM} = 17$ | $\varepsilon_{AOM} = 4$ | $\varepsilon_{AOM} = 17$ | AOM |
| 1 | 41.1 | – | 35.1 | – | 5.9 | 64.7 |
| 2 | 158.5 | 51.2 | 25.6 | 107.4 | 132.9 | 77.7 |
| 3 | 36.0 | – | 20.8 | – | 15.3 | 68.2 |
| 4 | 47.4 | 20.8 | 11.1 | 26.6 | 36.3 | 81.1 |

A. Integrated rates of AOM and OC (mmol $m^{-2}$ $day^{-1}$) based on whole core incubation and DIC isotope mass balance. A range of rates is shown based on the published range of values for $\varepsilon_{AOM}$ in sediment environments (4–17‰; see text).
B. Integrated rates of AOM (mmol $m^{-2}$ $day^{-1}$) calculated by integrating estimates of depth-specific rates (every 2 cm) based on batch incubations at 20°C, 5°C and 90°C across the measured temperature profiles of the whole core incubations. Integration was done using the trapezoidal rule.
C. Average volumetric rates of AOM and OC (nmol $cc^{-1}$ $day^{-1}$) in the whole core incubation calculated as in A.
D. Average volumetric rates of AOM (nmol $cc^{-1}$ $day^{-1}$) calculated as in B.

estimates to selected parameters, in particular the kinetic isotope effect by AOM ($\varepsilon_{AOM}$), are considered in the discussion.

### *ANME-1a abundance across temperature gradient in continuous flow incubations*

Via quantitative PCR, 16S ssu rRNA genes allied to the ANME-1a group of ANMEs were detected in virtually all core strata (discretely sampled every 2.5 cm from top to bottom, Fig. 3). ANME-1a abundance was quantified (copies g $sed^{-1}$) in subsamples from all four flow-through incubations, with 7 to 10 vertical horizons (every ~ 2.5 cm) measured in each core. The greatest abundance of ANME-1a copies were detected in the lower temperature horizons (26.6–35.5°C), ranging from $8.65 \times 10^3$ to $1.42 \times 10^5$ copies g $sed^{-1}$. Intriguingly, the lowest abundance of ANME-1a occurred at mid-range temperatures in

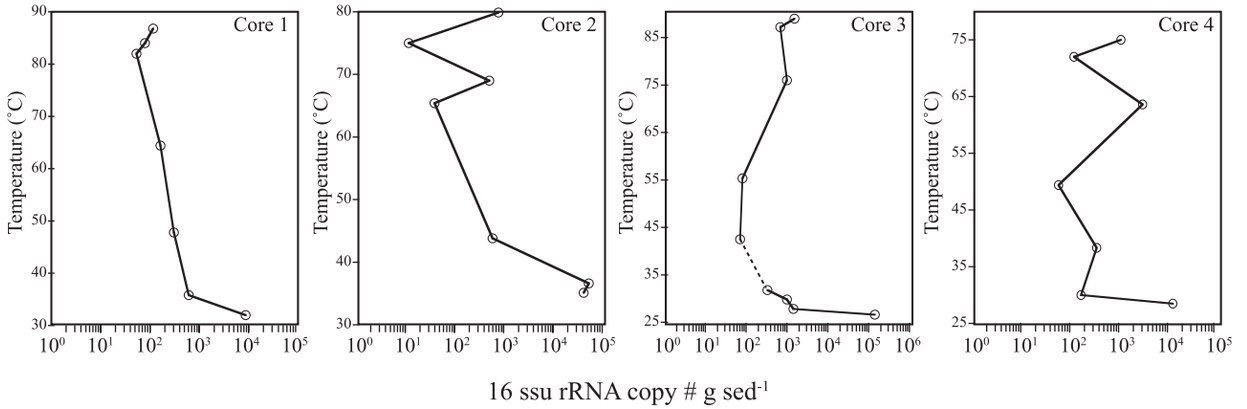


**Fig. 3.** Cell densities of ANME-1 anaerobic methanotrophic ribotypes as determined via quantification of 16 ssu rRNA gene copies per gram sediment. Data are shown versus sediment temperature from all flow-through incubator cores (see text for details). DNQ = rRNA gene copies were below our detection limits (100 copies per gram sediment). ANME-2c was not detected in any sediment core or horizon. Dotted line represents sediment interval that did not amplify due to inhibition. Note that highest temperatures are toward the top. Note that differences in sediment column heights result in variations in sample location with respect to temperature.

all sediment cores, with notable increases in ANME-1a abundance (Fig. 3) at higher temperatures in Core 2 ($8.81 \times 10^2$ ANME-1a copies g sed$^{-1}$ at 80°C), Core 3 ($1.53 \times 10^3$ ANME-1a copies g sed$^{-1}$ at 89°C) and Core 4 ($3.09 \times 10^3$ and $1.12 \times 10^3$ ANME-1a copies g sed$^{-1}$ at 63.6°C and 75°C respectively). In addition, total microbial density decreased from low to high temperature strata in the flow-through incubations, from approximately $5.7 \times 10^6$ to $3.1 \times 10^5$ cells ml$^{-1}$ from low to high temperature strata respectively (Table S1). These results suggest a higher relative abundance of ANME-1a with respect to total microbial cell density in those higher temperature sediments. ANME-2 ribotypes were not detected in any strata via qPCR. While the abundances presented above provide reasonable estimates of cell number, they should not be viewed as data on the absolute density of ANMEs as we do not yet know the number of 16 ssu rRNA gene copies per genome.

Observations via FISH corroborate that ANME-1a archaea, and not ANME-2, were present throughout all sediment horizons of all cores (Fig. S1). Moreover, bacteria allied to the *Desulfosarcina-Desulfococcus* group commonly associated with ANMEs were only observed in the lower temperature sediments (20°C and 50°C), and were not observed in sediments incubated at 90°C.

### *Phylogenetic diversity and distribution in sediments from continuous flow incubations*

A total of 19 010 archaeal sequences was generated via pyrosequencing of a segment of the 16 small subnit (ssu) rRNA gene from Core 2 sediments incubated at ~ 52°C (Fig. 4B; note that archaeal sequences from the 90°C sediments are not presented here due to issues with primer bias. Euryarchaeotal sequences were predominantly allied to *Thermoplasmata*, *Methanomicrobia*, *Thermococci*, *Archaeoglobi* and *Halobacteria* in decreasing abundance (25%, 17%, 8.4%, 5.1% and 2.3% respectively). Over 11.2% of sequences were allied to ANME-1a ribotypes and phylogenetically clustered with ANME-1a recovered from cold and warm marine sediments (Fig. S2). Other ribotypes also formed a unique clade within the ANME-1, which we have denoted as ANME-1c (Fig. S2). Other methanogen-like archaea were also recovered, primarily allied to *Methanosarcinales* (Fig. 4B).

A total of 7633, 5827 and 7290 bacterial sequences were also generated via pyrosequencing of DNA from Core 2 sediments incubated at 35°C, 44°C and 90°C respectively (the 44°C sample was proximal to the sediments analysed for the archaeal amplicon pool described above). The majority of sequences from both libraries were allied to the *Proteobacteria*, *Firmicutes*, *Actinobacteria* and *Bacteriodetes* at 54%, 34%, 2.2% and 2.1% of sequences at 35°C; 20.4%, 43.1%, 6.78% and 17.93% at 44°C and 39%, 45%, 4.4% and 2.6% of sequences at 90°C respectively (Fig. 4A). Among the *Proteobacteria*, sequences allied to known sulfate reducing *Deltaproteobacteria* were detected at 35°C and 43°C, comprising approximately 5% and 0.6% of the *Proteobacterial* sequences. Nearly all these sequences were allied to the genus *Desulfobulbus*, which is frequently observed in association with ANME in marine environments (Pernthaler *et al*., 2008).

### *AOM and SR rates as a function of sediment depth and temperature via batch incubations*

Batch radiotracer incubations revealed that temperature exerted a strong influence on AOM and SR rates (Fig. 5). Maximum volumetric AOM rates were observed at 55°C (234 ± 152 nmol cc$^{-1}$ day$^{-1}$, $n = 3$), while maximum SR rates were observed at both 20°C and 55°C (~ 100 nmol cc$^{-1}$ day$^{-1}$; $n = 3$). Notably, at 90°C, substantial AOM rates were observed (162 ± 5 nmol cc$^{-1}$ day$^{-1}$), while SR rates were below our limits of detection (~ 10 pmol cc$^{-1}$ day$^{-1}$). Larger differences observed among some of the replicates is likely due to the persistence of aggregates in these sediments, which were extremely difficult to disrupt and prevented complete homogenization.

In general, AOM and SR rates were also higher in sediments recovered from shallower horizons *in situ* (0–8 cm), where cell densities were highest (Table S1). While AOM rates in the deepest two layers (8–12 cm and 12–18 cm) were lower than the uppermost layers for the 55°C and 90°C batch incubations, no differences were observed in AOM rates among samples across depth incubated at 20°C (Fig. 5). SR rates were highest in the 4–8 cm layer and were not detected in sediments recovered from depths below 8 cm in the pushcores, regardless of incubation temperature.

## Discussion

Anaerobic oxidation of methane, and its relationship to SR, has been widely studied in many low-temperature, organic-rich marine sedimentary environments including cold seeps, hydrate-hosted sediments, brine pools, mud volcanoes and coastal shelf sediments (for review see Knittel and Boetius, 2009). Despite observations of high $CH_4$ fluxes from many hydrothermal systems (including sediment-hosted vents, e.g. Lilley *et al*., 1993; Seewald *et al*., 1994; Cruse and Seewald, 2006; Wankel *et al*., 2011), relatively little is known about the nature of AOM in high temperature environments and the potential role of AOM in the regulation of $CH_4$ and DIC fluxes to the deep

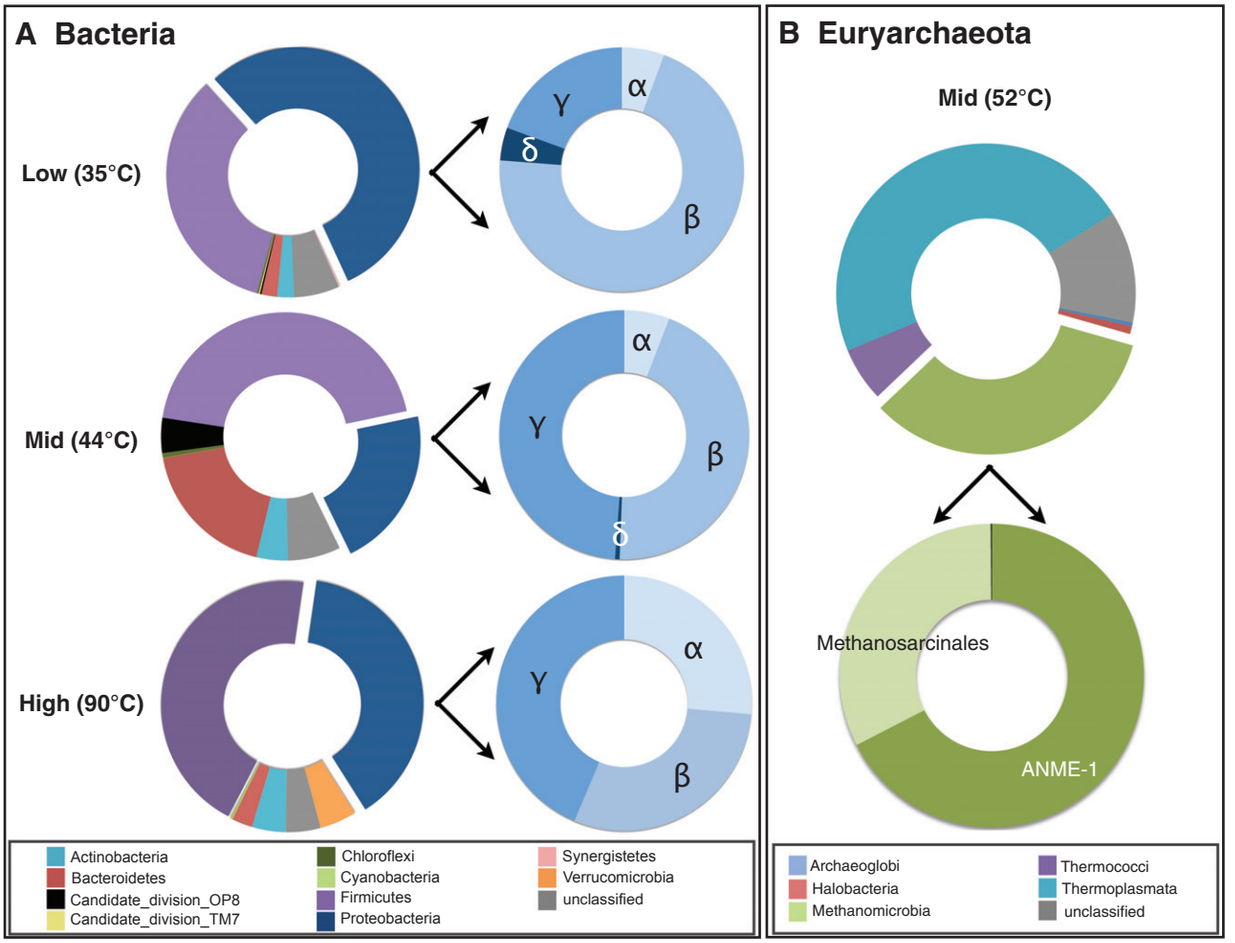


**Fig. 4.** A. Bacterial community diversity as determined from massively parallel sequencing of DNA recovered from low (~ 35°C), middle (~ 44°C) and high (~ 90°C) temperature flow-through reactor sediments (see text for details). Pie charts show the taxonomic breakdown of sequences at the domain and phyla level. Legend indicates operational taxonomic units, defined as sequences sharing 80% nucleotide sequence identity.
B. Euryarchaeal diversity as observed in the mid-temperature (~ 52°C) flow-through reactor sediments. Pie charts show the taxonomic breakdown of sequences at the phyla and class level. Efforts to generate Euryarchaeal sequences from other temperatures were unsuccessful due to bacterial amplification in the archaeal library.

ocean. Gaps in our understanding of AOM at hydrothermal systems include knowledge of the magnitude of AOM rates, the relationship between AOM and SR in hydrothermal systems, the composition of the anaerobic methanotrophic community, and the influence of temperature, fluid advection and fluid or sediment organic matter content on net AOM and SR rates. The data presented here reveal substantial AOM rates in hydrothermal vent sediments at temperatures from 20°C to 90°C, and suggest that AOM rates in metalliferous, hydrothermal sediments are elevated due in part to higher temperatures and advective fluid delivery. These data further demonstrate that AOM at higher temperatures is uncoupled from sulfate reduction and may be linked to reduction of mixed valence iron oxides. Our results indicate that AOM in this hydrothermal system is most likely mediated by ANME-1 phylotypes, as other known ANMEs were not detected in our community analyses or via qPCR or FISH. Equally important, the high contribution of AOM to the DIC pool establishes the significance of this process to carbon fluxes from hydrothermal sediments. These and other observations are discussed in detail below.

The AOM rates calculated from our flow-through incubations are among the highest reported for gas hydrate-free sediment and are similar in magnitude to those observed in the sulfate-methane transition zone of organic-rich sediments in coastal settings (e.g. Alperin *et al.*, 1988; Hoehler *et al.*, 1994; Girguis *et al.*, 2003; Treude *et al.*, 2005; Parkes *et al.*, 2007; Knab *et al.*, 2008; Wegener *et al.*, 2008). AOM rates (and subsequently the efficiency of $CH_4$ removal by AOM) depends heavily on the nature of methane delivery, given the high

 

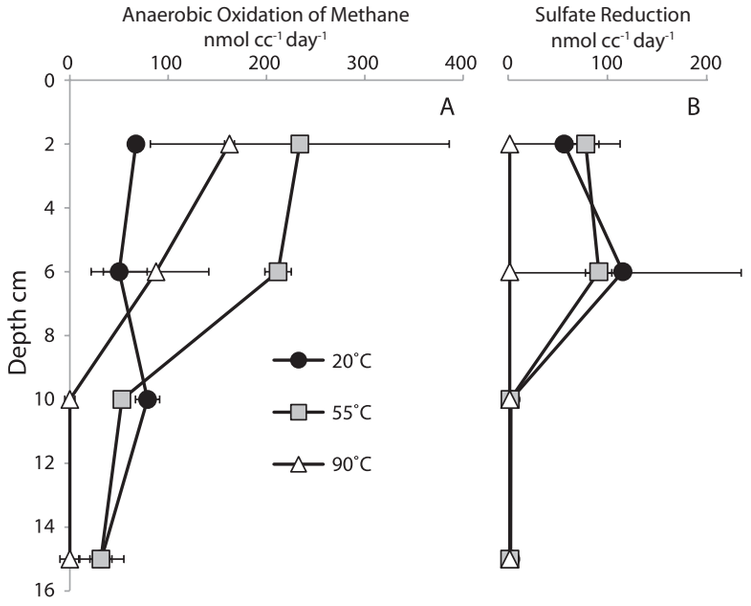


**Fig. 5.** (A) Anaerobic oxidation of methane rates, (B) sulfate reduction rates in batch incubations across sediment depths (0–4 cm, 4–8 cm, 8–12 cm and 12–18 cm sediment depths) at three temperatures. AOM and SR rates were determined by radiotracer analyses. Each point represents the average of three replicate rate measurements ± one standard deviation. AOM rates almost always exceeded SR rates and SR rates were undetectable at the highest incubation temperature. Note that all 90°C treatments resulted in no measurable SR and that no SR was detected in lower depths at all temperatures.

half-saturation constant ($K_m$) of methane for AOM (> 10 mM; (Nauhaus *et al*., 2005; 2007) and first-order nature of AOM with respect to $CH_4$ concentration (Knab *et al*., 2008). In diffusion-dominated systems, AOM rates can be on the order of pmol $cc^{-1}$ $day^{-1}$ with complete consumption of $CH_4$ occurring within a narrow sulfate-methane transition zone (e.g. Wellsbury *et al*., 2002). Conversely, in advection-dominated systems, AOM rates are generally higher (nmol $cc^{-1}$ $day^{-1}$ or higher) due to more rapid methane replenishment (Boetius and Seuss, 2004; Girguis *et al*., 2005; Lapham *et al*., 2008b; Solomon *et al*., 2009). Advective delivery of hydrothermal vent fluids through Middle Valley sediments likely supports elevated AOM rates *in situ* and plays an important role in our observed AOM rates during flow-through incubations.

The AOM and SR rates were also investigated via batch incubations across a range of temperatures (Fig. 5) to validate AOM rates observed in the flow-through incubations and to constrain the relationship between AOM and SR (discussed in more detail below). To enable comparison of the AOM rates from our batch and flow-through incubations, AOM batch incubation rates (at 20°C, 55°C and 90°C) were interpolated over the temperature profiles measured in the flow-through incubations. Depth-specific AOM rates were estimated over each sediment column and integrated (via trapezoidal integration, Table 2). The AOM rates measured in our batch reactions were two to seven times higher than the rates calculated from our flow-through incubations (Table 2), although they are still comparable to those measured in cold seep sediments (e.g. Girguis *et al*., 2003; Joye *et al*., 2004; Treude *et al*., 2005). A number of explanations could account for the observed differences in rates between the batch and column experiments. Sediment heterogeneity, which is extremely high in these settings, could explain the variability observed among the sediments that were used in batch experiments or continuous flow reactors. Alternatively, the duration of the flow-through incubations could have led to changes to the ANME community relative to those in the batch incubations. While the role of these factors in the observed variability cannot be discounted, we also suggest that the discrepancy may be due to lateral heterogeneity within the continuous flow bioreactors, due to channelization and flowpath heterogeneity within the sediments. Formation of channels was observed during the course of the experiments, which occurred partially due to $CH_4$ ebullition (see *Results*). Flowpath heterogeneity is a ubiquitous attribute of advective flow through sediments, and the inherent sediment heterogeneity (e.g. grain size) inevitably leads to small-scale flow channelization within sediments (e.g. Torres *et al*., 2002; Mahadevan and Mahadevan, 2010). Such channelization would result in geochemical, thermal and biological heterogeneity *in situ* as well as in our flow-through incubations. In advective systems, rapid fluid movement through sediments leads to a reduced residence time and thus a net reduction in the alteration of the fluid composition (in this case, due to methane oxidation). In such environments, the flux of fluid (and methane) through preferential flow channels operates as a fast 'bypass shunt' that leads to a decrease in 'oxidation efficiency' of the dissolved constituents (e.g. Sommer *et al*., 2006; Dale *et al*., 2008). Therefore, the physics of fluid movement, which controls fluid residence time within the biologically active zone (e.g. < ~ 120°C), plays a primary

role in dictating the efficiency of this methane sink. Thus, the lower rates of AOM measured in the core incubations – compared with the more homogeneous batch incubations – may more closely reflect *in situ* conditions observed in advective and heterogeneous regimes, including hydrocarbon seeps and sedimented hydrothermal vents systems.

The batch radiotracer incubations were also used to evaluate the relationship between AOM and SR over a range of environmentally relevant temperatures. AOM rates in sediments recovered from the upper 8 cm were highest at 55°C followed by 90°C. While this observed AOM rate maxima at 55°C is much higher than those observed for microbial communities in cold environments (Nauhaus *et al*., 2005; 2007; Meulepas *et al*., 2009), this is consistent with other recent studies of high temperature AOM in Guaymas Basin sediments with rate maxima between 50°C and 60°C (Kallmeyer and Boetius, 2004; Holler *et al*., 2011).

Most notably, there was a distinct shift in the ratio of AOM to SR among our batch experiments with increasing temperature, suggesting a change in the relationship between AOM and SR. Previous studies have demonstrated active SR in high temperature hydrothermal vent sediments such as the organic-rich sediments found in Guaymas Basin (Jorgensen *et al*., 1992; Kallmeyer and Boetius, 2004). In all of our 90°C incubations of Middle Valley sediments, however, no SR was detected, despite ample available sulfate and modest rates of AOM (Fig. 5). Congruent with the absence of SR at high temperatures was the lack of known SRB in the library of sequences recovered from higher temperature sediments (Fig. 4A), the lack of ANME-associated SRB visualized via FISH (Fig. S2) and the lack of dissimilatory (bi)sulfite reductase (*dsrA*) amplification at higher temperatures (not shown). Only the 20°C batch incubations of upper 8 cm sediments exhibited AOM : SR ratios that were consistent with the canonical stoichiometry of AOM : SR (e.g. 1:1, Hoehler *et al*., 1994). In general, stoichiometric ratios of DIC production to SR greater than 1 imply an increased contribution by sediment organic carbon oxidation (in which oxidation of $CH_2O$ by SR would yield a ratio ~ 2), and the ratio of DIC production to SR has been used to partition the relative coupling of SR to anaerobic oxidation of either sediment organic carbon or methane in diffusion-dominated porewater environments (Burdige and Komada, 2011). Surprisingly, however, in our batch experiments rates of AOM exceeded SR by a factor of 2 to 465 (when SR was quantifiable) at elevated temperatures. When a stoichiometric 'de-coupling' of AOM and SR has been noted in previous studies, SR has typically been observed in excess of AOM (e.g. global median estimate of SR : AOM = 10.7:1; Bowles *et al*., 2011), which occurs where the oxidation of other organic compounds support SR (Joye *et al*., 2004; Bowles *et al*., 2011). Our data reveal a striking uncoupling of AOM and SR, in which AOM rates are vastly greater than SR. These data clearly demonstrate that the canonical stoichiometry of AOM and SR is not characteristic of AOM at the higher temperatures and fluid composition found in these hydrothermal sediments.

The absence of detectable SRB and measurable SR and the presence of ANME and active AOM in the 90°C batch incubations suggest that AOM is coupled to the reduction of other electron acceptors. Indeed, recent studies have documented the coupling of AOM to the reduction of other terminal electron acceptors, such as nitrate or nitrite (Raghoebarsing *et al*., 2006) and/or reactive minerals including Mn and/or Fe oxides (Beal *et al*., 2009; Ettwig *et al*., 2010). Acid extractions from these sediments revealed substantial concentrations of oxidized iron (Fe, up to 67 mmol per g dry sediment) within the sediment cores obtained from the same site at Middle Valley (0 to 20 cm) (data not shown). Further, X-ray absorption spectroscopy (XAS) confirmed the presence of oxidized Fe in the sediments below 6 cm, as illustrated by a shift in the energy of the inflection point for the X-ray Absorption Near Edge Structure (XANES) spectra with depth (see Fig. S3). Fitting of the extended region of the XAS spectra [the Extended X-Ray Absorption Fine Structure (EXAFS) region] identified the mixed Fe(II)/Fe(III) phase green rust (as GR2, sulfate) as the likely Fe(III)-bearing phase (~ 32 mole %) within these sediments (6–9 cm). Green rust is a reactive transient Fe oxide phase, commonly linked to the redox cycling of lepidocrocite, a mineral phase that has previously been observed in Middle Valley sediments (Goodfellow and Blaise, 1988; Ames *et al*., 1993). Green rust may form as a product of microbial reduction of lepidocrocite (O'Laughlin *et al*., 2007) or as an intermediate during Fe(II) oxidation to lepidocrocite.

While a mechanistic characterization of AOM supported by microbial reduction of lepidocrocite or green rust-like phases fell beyond the scope of this study, bacterial sequences from 90°C in the flow-through incubations revealed that members of the *Verrucomicrobia*, which include putative metal-reducing phylotypes (Gremion *et al*., 2003), were abundant in the highest temperature strata (Fig. 4A). This is also consistent with previous studies of AOM indicating that *Verrucomicrobial* phylotypes were associated with iron- and manganese-dependent AOM communities in a low temperature environment (Beal *et al*., 2009). In fact, under conditions typical of Middle Valley sediments (Cruse *et al*., 2008), coupling of AOM with reduction of the mixed valent Fe oxide phase green rust (GR2, sulfate) (see Fig. S3), for example, would yield a Gibbs free energy of –203 kJ per mole $CH_4$. Future studies should aim to discern the precise role of these phylotypes in AOM dynamics in hydrothermal sediments.

The predominance of ANME-1 phylotypes and absence of other known ANMEs in the flow-through incubations, as assessed via massively parallel pyrosequencing and qPCR, suggest that ANME-1a are the primary phylotype responsible for AOM in Middle Valley sediments (as these libraries are based upon PCR amplification of 16 ssu rRNA genes, library abundance coarsely represents a group's abundance in the community, but should not be construed as truly quantitative). The presence, and even increased abundance with respect to total microbial biomass, of ANME-1a at elevated temperatures (Fig. 3) highlights their importance in hydrothermal sediment methane cycling. Intriguingly, phylogenetic analyses of the archaeal community at 43°C revealed ANME-1 sequences that cluster as a unique subgroup (named ANME-1c herein; Fig. S2) which appear to be more closely related to other ANME-1 than to recently detected high-temperature ANME sequences found in Guaymas Basin (e.g. 'ANME-1Guaymas'; Biddle *et al*., 2011). Based on cursory phylogenetic analyses of the ANME-1 Guaymas sequences, it is unlikely that they are highly similar to the ANME-1c group described herein. Further studies, however, should aim to determine if these ANME-1c ribotypes are unique to Middle Valley and further explore the relationship among the high-temperature ANME phylotypes.

Much of the previous biological and geochemical evidence for AOM at high temperature has revealed activity of ANMEs in the hydrothermal vent sediments of the Guaymas Basin (> 30°C). The Guaymas Basin is characterized by high amounts of organic matter (e.g. 2–4%) and is in many ways more similar to hydrocarbon cold seeps than organic-poor hydrothermal vents found along the global mid ocean ridge system. Indeed, the differences in SR rates from our study (which are low) compared with the higher SR rates of Guaymas Basin sediments (Jorgensen *et al*., 1992) highlight the geochemical and microbiological distinctions between mid-ocean ridge vents (e.g. the East Pacific Rise, Mid-Atlantic Ridge and Juan de Fuca Ridge) and sedimented hydrothermal ridge systems (e.g. Guaymas Basin, the Red Sea and the Sea of Japan). Nonetheless, the observed high AOM rates in the absence of SR from this study demonstrate the potential for low organic carbon, high-temperature environments to support thermophilic AOM coupled to electron acceptors other than sulfate.

Our isotope mass balance reveals for the first time that AOM contributes substantially to the DIC flux from metalliferous, hydrothermal sediments. Depending on the value of $\varepsilon_{AOM}$ the contribution of AOM relative to OC oxidation is variable (Fig. 2): lower values of $\varepsilon_{AOM}$ (4‰) yield higher proportions of DIC production by AOM, while higher values of $\varepsilon_{AOM}$ (17‰) give lower estimates of the contribution by AOM to DIC flux [values chosen here reflect a range of AOM observed in sedimentary environments (Alperin and Hoehler, 2009)]. We determined that AOM could readily account for 16% to 86% of DIC production, and in some cases up to ~ 100% of DIC production (e.g. Core 1). In comparison, DIC production by OC oxidation (5.9 to 132.9 nmol $cc^{-1}$ $day^{-1}$) represented on average ~ 16%, ~ 82%, ~ 36% and ~ 74% of DIC production in Cores 1 through 4, respectively (Table 1). While all four cores were similar in total organic carbon (Table S1), Core 2 exhibited substantially higher organic carbon oxidation rates (up to 138.3 nmol $cc^{-1}$ $day^{-1}$; Table 2, Fig. 2). Among all four cores at all depths, the %OC and $\delta^{13}C$ values of the sediment organic carbon pool were also remarkably homogenous (%OC = 0.50 to 0.34 and $\delta^{13}C = -29‰ \pm 0.4$; Table S1). Therefore, the endogenous carbon in Core 2 was most likely more labile, which would not necessarily be apparent in quantification of total organic carbon. Despite apparently high variability in the OC oxidation rates, the relative contribution to DIC production by AOM was of similar magnitude and may even account for the majority of DIC production in some diffuse flow sediments of Middle Valley. These findings emphasize the importance of AOM in carbon cycling in hydrothermal vent sediments and underscore the need for similar characterization within other environments.

Both sediment temperature and organic matter content are major factors that control AOM-derived DIC production relative to organic matter oxidation. For example, Cruse and Seewald (2006) showed that $\delta^{13}C$ values of DIC in hydrothermal fluids from Middle Valley were low relative to seawater ($\delta^{13}C = -27.8‰$ to $-20.7‰$), suggesting a pronounced input of low $\delta^{13}C_{DIC}$, although the contribution of AOM to the $\delta^{13}C_{DIC}$ in this hydrothermal system was concluded to be only modest. In contrast to our results, Cruse and Seewald (2006) focused on higher temperature fluids (186–281°C) and the observed $\delta^{13}C_{DIC}$ likely reflects the abiotic hydrothermal alteration of organic matter with no abiotic methane oxidation since methane is stable at elevated temperatures. In cooler regimes, such as low-velocity 'diffuse' flows with more prevalent microbial activity, fluid $\delta^{13}C_{DIC}$ will likely reflect an increased contribution of biological DIC production (including both AOM and heterotrophy). Both the lower *in situ* sediment temperatures and flow velocities typical of low-velocity diffuse flows (as in the cores collected for this study) are more conducive to higher biological activity and their associated influence on DIC flux. In addition to temperature regime, sediment organic matter content in these Middle Valley sediments – similar to open ocean sediments in regions of modest productivity at ~ 0.4% total organic carbon (Emerson and Hedges, 1988) – will also play an important role in the relative importance of AOM to DIC production. As previously mentioned, the hydrothermally-hosted organic-rich sediments of the

Guaymas basin exhibit high potential AOM rates up to 1.2 μmol $g_{dw}^{-1}$ $day^{-1}$ (Holler *et al.*, 2011) and contain an unusually high sediment organic carbon content at ~ 2.5% (Seewald *et al.*, 1994). Such differences in sediment organic content undoubtedly contribute to the relative importance of AOM to DIC flux and are indicative of the distinctions in microbial community composition and activity in addition to the relationships among AOM, OC oxidation and SR in hydrothermally influenced sediments. In light of the role that diffuse flows play in governing geochemical flux from vents and potentially contributing to more than half of total geochemical flux from hydrothermal systems (Proskurowski *et al.*, 2008; Wankel *et al.*, 2011), AOM could exert an important influence on the diffuse flux of both methane and DIC from hydrothermal systems.

### *Conclusions*

These collective results underscore the importance of AOM in hydrothermal methane cycling by demonstrating substantial AOM rates at temperatures up to at least 90°C and by highlighting the relative importance of AOM in DIC production from sediments of modest organic carbon content. Furthermore, these data reveal a distinct decoupling of AOM from SR at high temperature and suggest that AOM may be coupled to the reduction of other mixed valent Fe oxides, such as green rust, at the temperatures and conditions examined herein. Expanding the extent of the previously unknown ANME-1c phylotype is of great interest as this group may be specifically adapted to organic-poor hydrothermal systems and may play a more primary role in mediating AOM coupled to the reduction of other electron acceptors in these types of environments. In concert, these results extend our understanding of the nature of high temperature methane biogeochemistry and suggest that AOM may play a central role in regulating biological DIC fluxes to the deep ocean from the organic-poor, metalliferous sediments of the global mid-ocean ridge hydrothermal vent system.

## Experimental procedures

### *Sediment collection*

Pushcores (20–30 cm sediment height, 6.35 cm ID, 0.32 cm sleeve thickness, made of polyvinylchloride which is highly resistant to oxygen permeation) of unconsolidated sediment were collected during an expedition with the *DSV Alvin* and *R/V Atlantis* in July 2007 from the Chowder Hill hydrothermal vent field in Middle Valley (48°27.25N, 128°42W) at 2428 m depth. Sampling sites were chosen based on the observation of 'shimmering water' (e.g. the 'schlieren' effect) that results from mixing of fluids with different densities, *in situ* temperature measurements made with *DSV Alvin*, and presence of microbial mat atop the sediments. Pushcores were collected from areas where sediments exhibited temperatures between ~ 2°C and 35°C in the upper 5 cm, and between 75°C and 150°C at 10 cm sediment depth. Upon retrieval, cores were sealed on board ship and refrigerated for transport to the laboratory. To prevent disruption of sediment structure and the associated microbial communities prior to incubation on the continuous-flow bioreactors, no samples were collected initially from the intact sediment cores. Upon return to the lab, the overlying water in the sediment cores was replaced weekly with fresh, filter-sterilized seawater prior to the initiation of the experiments.

### *Thermal gradient, continuous flow bioreactor setup*

Four intact sediment cores were loaded onto the experimental incubation manifold and irrigated with simulated vent effluent beginning in December 2007 (Fig. 1). Our simulated hydrothermal vent fluid was generated by continuous equilibration of 0.2 μm filter-sterilized seawater (~ 28 mM $SO_4^{-2}$) with a continuous flow of $H_2S$ and $CH_4$ gas to achieve dissolved concentrations of 0.97 mM and 2.8 mM respectively. The provision of sulfide ensured that the sediments remained at reducing conditions and that any trace contaminant oxygen was rapidly removed. The simulated vent effluent entered the reactor system through a gastight fitting at the core base using a high precision peristaltic pump. Flow rates were maintained at 28 ml $day^{-1}$ generating a linear flow velocity of ~ 0.9 cm $day^{-1}$ upward through the sediments. All cores were maintained in a thermal gradient through the use of silicone heating pads wrapped around the lower 8 cm of the core (Fig. 1), which provided a stable temperature gradient ranging from 90°C at the bottom to ~ 22°C near the top of each core sleeve, similar to gradients observed *in situ*. Prior to collection of the samples analysed herein, the flow-through core system in operation was for ~ 200 days (approximately eight turnovers of the pore fluid volume within the cores) to ensure steady-state conditions were achieved. After this incubation period, sediment temperature was determined by drilling into the side of each core, and inserting a digital temperature probe (ThermoFisher). Next, fluids and sediments were collected and analysed as described below for analyses.

### *Geochemical and isotopic measurements*

The geochemical and isotopic composition of inflow and outflow fluids was monitored daily in the flow-through incubations. DIC was measured from 1 ml of fluid injected anaerobically into pre-flushed 12 ml exetainers containing 1 ml of $H_3PO_4$ to evolve DIC as $CO_2$ for analysis via an isotope ratio mass spectrometer (IRMS). DIC concentrations were quantified based on integrated IRMS peak areas and periodic analysis of a calibrated $NaHCO_3$ standard. Analyses of DIC and methane concentration and stable isotopic composition (reported using δ notation: $\delta^{13}C_{DIC}$ (‰ vs. VPDB) = $[(^{13}R_{DIC}/^{13}R_{VPDB}) - 1]*1000$, where $^{13}R = {}^{13}C/{}^{12}C$) were analysed using a GasBench coupled to a Delta Plus

IRMS (ThermoFinnigan) at Harvard University (with inline oxidation of $CH_4$ to $CO_2$ prior to analysis), with a precision of 0.2‰ and ± 0.1 mM for $\delta^{13}C_{DIC}$ and total DIC concentration respectively, and 0.5‰ and ± 7% for dissolved $CH_4$ concentration respectively. After oven drying (50°C) and acidification, total bulk sediment organic carbon (OC) content and $\delta^{13}C_{OC}$ was measured using a Carlo Erba 1500 elemental analyser coupled to a Delta Plus IRMS (with a precision of 0.2‰ for $\delta^{13}C$ and 0.2% for %C). Methane concentration and stable carbon isotopic composition ($\delta^{13}C_{CH4}$) were measured daily from 4 ml of fluid anaerobically injected into a pre-flushed 12 ml exetainer and analysed at the UC Davis Stable Isotope Facility using a GasBench and Delta Plus IRMS. After equilibration at room temperature, headspace gas was flushed through a sampling loop, allowing for a fixed volume (100 µl) of gas to be routed through an oxidation furnace in which $CH_4$ was quantitatively converted to $CO_2$ prior to IRMS analysis. Integrated IRMS peak areas varied based on the headspace $CH_4$ content, which was related directly to dissolved $CH_4$ concentration using Henry's Law. Based on periodic analyses of methane standards with known concentration and isotopic composition, $\delta^{13}C_{CH4}$ reproducibility was ± 0.5‰.

### *DNA extractions and molecular microbiological analyses*

At the conclusion of the flow-through incubations, sediments were extruded and sectioned at 2 cm intervals from all cores. Total genomic DNA was extracted with the Powersoil DNA extraction kit (MoBio, San Diego, CA) modified to improve yields and eliminate potential metalliferous inhibitors of PCR downstream (see Supporting information; Webster *et al*., 2003). DNA recovered from Core 2 was used as template for massively parallel 454 sequencing (Roche Life Sciences). The resulting sequences were cleaned, aligned and subject to phylogenetic analyses. Sequences resulting from these analyses have been submitted to National Center for Biotechnology Information's GenBank (accession numbers JN907017 – JN934261). DNA recovered from all sediment horizons were used as template for quantification of ANME-1a and ANME-2 ribotypes. Sediment subsamples were also preserved for fluorescent *in situ* hybridization as well as cell counts. Briefly, cell counts were obtained by filtering, staining with SYBRI and counting at 100X with a gridded ocular (see Supporting information; D'Hondt *et al*., 2004).

### *Radiotracer rate measurements of batch incubations*

In parallel to the flow-through core incubations, sediment cores collected from the same sites were sectioned at 4 cm intervals, homogenized, and incubated in crimp sealed vials with the same simulated hydrothermal vent water used in the flow-through bioreactor in December 2007. Triplicate sediment samples from four depth horizons (0–4, 4–8, 8–12 and 12–18 cm) were incubated at three different temperatures (20°C, 55°C and 90°C) for 72 h prior to addition of radiotracer to quantify AOM and SR rates (see Supporting information; Canfield *et al*., 1986; Onstad *et al*., 2000; Joye *et al*., 2004; Orcutt *et al*., 2005).

### *DIC stable isotope mass balance*

A simple steady-state isotope mass balance model allowed for partitioning of the proportion of DIC production attributable to the anaerobic oxidation of either methane (AOM) or sediment organic carbon (OC). The model is based on the following assumptions: (i) all processes are operating at 'steady state,' such that mass balance is satisfied; (ii) AOM (independent of the oxidant) results in the stoichiometric conversion of $CH_{4(aq)}$ into $HCO_3^-$; (iii) the carbon isotope fractionation factor for AOM ($\varepsilon_{AOM}$) ranges between 4‰ to 17‰ [based on studies of AOM in sediments (Alperin and Hoehler, 2009)]; (iv) the carbon isotopic composition of the indigenous sediment organic carbon does not change substantially over the course of the experiment; (v) the isotopic composition and concentrations of the influent DIC and $CH_4$ are known and do not change and (vi) the size of the sediment biomass pool does not change substantially. Based on these conditions, the DIC flux from the effluent ($F_{out}$) is equal to the input flux ($F_{in}$; i.e. background seawater DIC) plus the contribution to DIC flux from the anaerobic oxidation of sediment organic carbon (OC) and/or methane (AOM):

$$F_{out} = F_{in} + \mathrm{AOM} + \mathrm{OC} \quad (1)$$

An isotope mass balance for $\delta^{13}C_{DIC}$ was constructed similarly according to the following equation:

$$F_{out} * \delta^{13}C_{out} = (F_{in} * \delta^{13}C_{in}) + [\mathrm{AOM} * (\delta^{13}C_{CH4} - \varepsilon_{AOM})] + (\mathrm{OC} * \delta^{13}C_{org}) \quad (2)$$

where $\varepsilon_{AOM}$ is the isotopic fractionation of $CH_4$ during oxidation by AOM (4–17‰ (Alperin and Hoehler, 2009), $\delta^{13}C_{in}$ is the isotopic composition of the influent seawater DIC (+3.4‰) and $\delta^{13}C_{org}$ is the average measured $\delta^{13}C$ of sediment organic matter (equal here to –29.0 ± 0.4‰). No fractionation was assumed to occur during the anaerobic oxidation of native organic matter. By combining equations 1 and 2, the fluxes of DIC produced by either AOM or OC were calculated and expressed per volume of sediment (Table 1). The range of $\varepsilon_{AOM}$ values (4–17‰) selected for AOM rate calculations from previous studies excludes recent higher estimates of $\varepsilon_{AOM}$ for ANME-2 and ANME-3 (Holler *et al*., 2009) because our quantitative phylogenetic analysis suggested ANME-1a is the dominant AOM-mediating group. Consequently, use of a range of $\varepsilon_{AOM}$ values in our model yields a range of the estimated proportion of AOM (and OC) to the DIC flux. Calculated rates of AOM ranged from 20.8 to 51.2 nmol $cc^{-1}$ $day^{-1}$ (at $\varepsilon_{AOM}$ = 4‰) and 11.1 to 35.1 nmol $cc^{-1}$ $day^{-1}$ (at $\varepsilon_{AOM}$ = 17‰).

## Acknowledgements

We are grateful for the expert assistance of the R/V *Atlantis* crews and the pilots and team of the DSV *Alvin* for enabling the collection of temperature data and sediment cores used in our experiments. We thank Wil Leavitt, Chris Lentini, Adiari Vazquez-Rodriguez, Daniel Stolper, Tom Yu, John Melas-Kyriazi, Pengfei Song, Kristina Fontanez, Roxanne Beinart and Mark Nielsen for providing assistance with various aspects of the experiments, sample processing and/or data interpretation. We also thank Colleen Cavanaugh and

Andrew Knoll for their constructive input during the preparation of this manuscript. Portions of this research were carried out at the Stanford Synchrotron Radiation Lightsource, a national user facility operated by Stanford University on behalf of the US Department of Energy, Office of Basic Energy Sciences. The SSRL Structural Molecular Biology Program is supported by the Department of Energy, Office of Biological and Environmental Research, and by the National Institutes of Health, National Center for Research Resources, Biomedical Technology Program. Support for this research was provided in part by NSF MCB *0702504* and NASA ASTEP grant *0910169* to P. R. Girguis and NASA ASTEP grant *NNX07AV51G* to P. R. Girguis and Andrew Knoll.

*Author contributions*

S. D. W., P. R. G. and M. M. A. designed the research. S. D. W. and P. R. G. directed the *in situ* collections and measurements. S. D. W., D. T. J. and M. M. A. conducted the flow-through incubations and geochemical analyses. S. D. W. directed and analysed the carbon stable isotope analyses, mass balance and rate calculations. M. M. A. performed the molecular analyses. C. M. H. directed and analysed the XAS/EXAFS data collection and analyses. S. B. J. performed the radioisotope rate measurements and analyses. S. D. W., PRG, and M. M. A. wrote the manuscript with input from C. M. H., S. B. J. and D. T. J. The authors declare no conflict of interest.

## References

Alperin, M., and Reeburgh, W.S. (1985) Inhibition experiments on anaerobic methane oxidation. *Appl Environ Microbiol* **50:** 940–945.

Alperin, M., Reeburgh, W.S., and Whiticar, M. (1988) Carbon and hydrogen fractionation resulting from anaerobic methane oxidation. *Global Biogeochem Cycles* **2:** 279–288.

Alperin, M.J., and Hoehler, T.M. (2009) Anerobic methane oxidation by archaea/sulfate-reducing aggregates: 2. Isotopic Constraints. *Am J Sci* **309:** 958–984.

Ames, D.E., Franklin, J.M., and Hannington, M.D. (1993) Mineralogy and geochemistry of active and inactive chimneys and massive sulfide, Middle Valley, Northern Juan de Fuca Ridge: an evoloving hydrothermal system. *Can Mineral* **31:** 997–1024.

Beal, E.J., House, C.H., and Orphan, V.J. (2009) Manganese- and iron-dependent marine methane oxidation. *Science* **325:** 184–187.

Biddle, J.F., Cardman, Z., Mendlovitz, H., Albert, D., Lloyd, K.G., Boetius, A., and Teske, A. (2011) Anaerobic oxidation of methane at different temperature regimes in Guaymas Basin hydorthermal sediments. *ISME J* **6:** 1018–1031.

Boetius, A., and Seuss, E. (2004) Hydrate Ridge: a natural laboratory for the study of microbial life fueled by methane from near-surface gas hydrates. *Chem Geol* **205:** 281–310.

Boetius, A., Ravenschlag, K., Schubert, C.J., Rickert, D., Widdel, F., Gieseke, A., *et al*. (2000) A marine microbial consortium apparently mediating anaerobic oxidation of methane. *Nature* **407:** 623–626.

Bowles, M.W., Samarkin, V., Bowles, K.M., and Joye, S.B. (2011) Weak coupling between sulfate reduction and the anaerobic oxidation of methane in methan-rich seafloor sediments during *ex situ* incubation. *Geochim Cosmochim Acta* **75:** 500–519.

Burdige, D., and Komada, T. (2011) Anaerobic oxidation of methane and the stoichiometry of remineralization processes in continental margin sediments. *Limnol Oceanogr* **56:** 1781–1796.

Canfield, D.E., Raiswell, R., Westrich, J.T., Reaves, C.M., and Berner, R.A. (1986) The use of chromium reduction in the analysis of reduced inorganic sulfur in sediments and shales. *Chem Geol* **54:** 144–159.

Conrad, R. (2009) The global methane cycle: recent advances in understanding the microbial processes involved. *Environ Microbiol Rep* **1:** 285–292.

Coumou, D., Driesner, T., Geiger, S., Heinrich, C., and Matthai, S. (2008) The structure and dynamics of mid-ocean ridge hydrothermal systems. *Science* **321:** 1825.

Cruse, A., and Seewald, J.S. (2006) Geochemistry of low-molecular weight hydrocarbons in hydrothermal fluids from Middle Valley, northern Juan de Fuca Ridge. *Geochim Cosmochim Acta* **70:** 2073–2092.

Cruse, A., and Seewald, J.S. (2010) Low-molecular weight hydrocarbons in vent fluids from the Main Endeavor Field, northern Juan de Fuca Ridge. *Geochim Cosmochim Acta* **74:** 6126–6140.

Cruse, A.M., Seewald, J.S., Saccocia, P.J., and Zierenberg, R.A. (2008) Geochemistry of hydrothermal fluids from Middle Valley, northern Juan de Fuca Ridge: temporal variability, subsurface conditions and equilibration during upflow. In *Magma to Microbe: Modeling Hydrothermal Processes at Oceanic Spreading Centers*. AGU Monograph Series. Vol. 178. Lowell, R., Seewald, J.S., Metaxas, A., and Metaxas, M.R. (eds). Washington, DC, USA: American Geophysical Union, pp. 145–116.

D'Hondt, S., Jorgensen, B.B., Miller, D.J., Batzke, A., Blake, R., Cragg, B.A., *et al*. (2004) Distributions of microbial activities in deep subseafloor sediments. *Science* **306:** 2216–2221.

Dale, A.W., Regnier, P., Knab, N.J., Jorgensen, B.B., and Van Cappellen, P. (2008) Anaerobic oxidation of methane (AOM) in marine sediments from Skagerrak (Denmark): II. Reaction-transport modelling. *Geochim Cosmochim Acta* **72:** 2880–2894.

Emerson, S., and Hedges, J. (1988) Processes controlling the organic carbon content of open ocean sediments. *Paleoceanography* **3:** 621–634.

Ettwig, K.F., Butler, M.K., Le Paslier, D., Pelletier, E., Mangenot, S., Kuypers, M.M.M., *et al*. (2010) Nitrite-driven anaerobic methane oxidation by oxygenic bacteria. *Nature* **464:** 543–548.

Girguis, P.R., Orphan, V.J., Hallam, S.J., and DeLong, E.F. (2003) Growth and methane oxidation rates of anaerobic methanotrophic archaea in a continuous flow reactor bioreactor. *Appl Environ Microbiol* **69:** 5492–5502.

Girguis, P.R., Cozen, A.E., and DeLong, E.F. (2005) Growth and population dynamics of anaerobic methane-oxidizing archaea and sulfate-reducing bacteria in a continuous flow bioreactor. *Appl Environ Microbiol* **71:** 3725–3733.

Goodfellow, W.D., and Blaise, B. (1988) Sulfide formation and hydrothermal alteration of hemipelagic sediment in Middle Valley, Northern Juan de Fuca Ridge. *Can Mineral* **26:** 675–696.

Gremion, F., Chatzinotas, A., and Harms, H. (2003) Comparative 16S rDNA and 16S rRNA sequence analysis indicates that *Actinobacteria* might be a dominant part of the metabolically active bacteria in heavy-metal-contaminated bulk and rhizosphere soil. *Environ Microbiol* **5:** 896–907.

Hinrichs, K.-U., Hayes, J.M., Sylva, S.P., Brewer, P.G., and DeLong, E.F. (1999) Methane consuming archaebacteria in marine sediments. *Nature* **398:** 802–805.

Hoehler, T.M., Alperin, M., and Albert, D. (1994) Field and laboratory studies of methane oxidation in anoxic marine sediment: Evidence for a methanogen-sulfate reducer consortium. *Global Biogeochem Cycles* **8:** 451–463.

Holler, T., Wegener, G., Knittel, K., Boetius, A., Brunner, B., Kuypers, M.M.M., and Widdel, F. (2009) Substantial $^{13}C/^{12}C$ and D/H fractionation during anaerobic oxidation of methane by marine consortia enriched *in vitro*. *Environ Microbiol Rep* **1:** 370–376.

Holler, T., Widdel, F., Knittel, K., Amann, R., Kellerman, M.Y., Hinrichs, K.-U., *et al*. (2011) Thermophilic anaerobic oxidation of methane by marine microbial consortia. *ISME J* **5:** 1946–1956.

Iversen, N., and Jorgensen, B.B. (1985) Anaerobic methane oxidation rates at the sulfate methane transition in marine sediments. *Limnol Oceanogr* **30:** 944–955.

Jorgensen, B.B., Isaksen, M.F., and Jannasch, H.W. (1992) Bacterial sulfate reduction above 100°C in deep-sea hydrothermal vent sediments. *Science* **258:** 1756–1757.

Joye, S.B., Boetius, A., Orcutt, B.N., Montoya, J.P., Schulz, H.N., Erickson, M.J., and Lugo, S. (2004) The anaerobic oxidation of methane and sulfate reduction in sediments from Gulf of Mexico cold seeps. *Chem Geol* **205:** 219–238.

Kallmeyer, J., and Boetius, A. (2004) Effects of temperature and pressure on sulfate reduction and anaerobic oxidation of methane in hydrothermal sediments of Guaymas Basin. *Appl Environ Microbiol* **70:** 1231–1233.

Knab, N.J., Dale, A.W., Lettman, K., Fossing, H., and Jorgensen, B.B. (2008) Thermodynamic and kinetic control on anaerobic oxidation of methane in marine sediments. *Geochim Cosmochim Acta* **72:** 3746–3757.

Knittel, K., and Boetius, A. (2009) Anaerobic oxidation of methane: Progress with an unknown process. *Annu Rev Microbiol* **63:** 311–334.

Lapham, L.L., Chanton, J., Martens, C.S., Higley, P.D., Jannasch, H.W., and Woolsey, J.R. (2008a) Measuring temporal variability in pore-fluid chemistry to assess gas hydrate stability: development of a continuous pore-fluid array. *Environ Sci Technol* **42:** 7368–7373.

Lapham, L.L., Alperin, M., Chanton, J., and Martens, C.S. (2008b) Upward advection rates and methane fluxes, oxidation, and sources at two Gulf of Mexico brine seeps. *Mar Chem* **112:** 65–71.

Lilley, M.D., Butterfield, D.A., Olson, E.J., Lupton, J.E., Macko, S.A., and McDuff, R.E. (1993) Anomalous $CH_4$ and $NH_4^+$ concentrations at an unsedimented mid-ocean-ridge hydrothermal system. *Nature* **364:** 45–47.

Lloyd, K.G., Alperin, M.J., and Teske, A. (2011) Environmental evidence for net methane production and oxidation in putative ANaerobic MEthanotrophic (ANME) archaea. *Environ Microbiol* **13:** 2548–2564.

Mahadevan, A., and Mahadevan, L. (2010) Flow-induced channelization in a porous medium. *Engineering* **1:** 4.

Martens, C.S., and Berner, R.A. (1974) Methane production in the interstitial waters of sulfate-depleted marine sediments. *Science* **185:** 1167–1169.

Meulepas, R.J., Jagersma, C.G., Khadem, A.F., Buisman, C.J., Stams, A.J., and Lens, P.N. (2009) Effect of environmental conditions on sulfate reduction with methane as electron donor by an Eckernförde Bay enrichment. *Environ Sci Technol* **43:** 6553–6559.

Nauhaus, K., Boetius, A., Krüger, M., and Widdel, F. (2002) In vitro demonstration of anaerobic oxidation of methane coupled to sulphate reduction in sediment from a marine gas hydrate area. *Environ Microbiol* **4:** 296–305.

Nauhaus, K., Treude, T., Boetius, A., and Krüger, M. (2005) Environmental regulation of the anaerobic oxidation of methane: a comparison of ANME-1 and ANME-II communities. *Environ Microbiol* **7:** 98–106.

Nauhaus, K., Albrecht, M., Elvert, M., Boetius, A., and Widdel, F. (2007) In vitro cell growth of marine archaeal-bacterial consortia during anaerobic oxidation of methane with sulfate. *Environ Microbiol* **9:** 187–196.

O'Laughlin, E.J., Larese-Casanova, P., Scherer, M., and Cook, R. (2007) Green rust formation from the bioreduction of γ-FeOOH (lepidocrocite): comparison of several *Shewanella* spcies. *Geomicrobiol J* **24:** 211–230.

Onstad, G.D., Canfield, D.E., Quay, P.D., and Hedges, J.I. (2000) Sources of particulate organic matter in rivers from the continental USA: lignin phenol and stable carbon isotope compositions. *Geochim Cosmochim Acta* **64:** 3539–3546.

Orcutt, B.N., Boetius, A., Elvert, M., Samarkin, V., and Joye, S.B. (2005) Molecular biogeochemistry of sulfate reduction, methanogenesis and the anaerobic oxidation of methane at Gulf of Mexico cold seeps. *Geochim Cosmochim Acta* **69:** 4267–4281.

Orphan, V.J., House, C.H., Hinrichs, K.-U., McKeegan, K.D., and DeLong, E.F. (2001) Methane-consuming archaea revealed by directly coupled isotopic and phylogenetic analysis. *Science* **293:** 484–487.

Orphan, V.J., House, C.H., Hinrichs, K.-U., McKeegan, K.D., and DeLong, E.F. (2002) Multiple archael groups mediate methane oxidation in anoxic cold seep sediments. *Proc Natl Acad Sci USA* **99:** 7663–7668.

Parkes, R.J., Cragg, B.A., Banning, N., Brock, F., Webster, G., Fry, J.C., *et al*. (2007) Biogeochemistry and biodiversity of methane cycling in subsurface marine sediments (Skagerrak, Denmark). *Environ Microbiol* **9:** 1146–1161.

Pernthaler, A., Dekas, A.E., Brown, C.T., Goffredi, S.K., Embaye, T., and Orphan, V.J. (2008) Diverse syntrophic partnerships from deep-sea methane vents revealed by direct cell capture and metagenomics. *Proc Natl Acad Sci USA* **105**: 7052–7057.

Price, M.N., Dehal, P.S., and Arkin, A.P. (2010) FastTree 2 – approximately maximum-likelihood trees for large alignments. *PLoS ONE* **5**: 9490.

Proskurowski, G., Lilley, M.D., and Olson, E.J. (2008) Stable isotopic evidence in support of active microbial methane cycling in low-temperature diffuse flow vents at 9°50′ N East Pacific Rise. *Geochim Cosmochim Acta* **72:** 2005–2023.

Ragshoebarsing, A.A., Pol, A., van de Pas-Schoonen, K., Smolders, A.J.P., Ettwig, K.F., Rijpstra, I.C., *et al.* (2006) A microbial consortium couples anaerobic methane oxidation to denitrification. *Nature* **440:** 918–921.

Reeburgh, W.S. (1976) Methane consumption in Cariaco Trench waters and sediments. *Earth Planet Sci Lett* **28:** 337–344.

Reeburgh, W.S. (2007) Oceanic methane biogeochemistry. *Chem Rev* **107:** 486–513.

Rushdl, A., and Simonelt, B. (2002) Hydrothermal alteration of organic matter in sediments of the Northeastern Pacific Ocean: Part 1: Middle Valley, Juan de Fuca Ridge. *Appl Geochem* **17:** 1401–1428.

Schouten, S., Wakeham, S.G., Hopmans, E.C., and Damste, J.S.S. (2003) Biogeochemical evidence that thermophilic archaea mediate the anaerobic oxidation of methane. *Appl Environ Microbiol* **69:** 1680–1686.

Seewald, J.S., Seyfried, W.E., Jr, and Shanks, W.C., III (1994) Variations in the chemical and stable isotope composition of carbon and sulfur species during organic-rich sediment alteration: an experimental and theoretical study of hydrothermal activity at Guaymas Basin, Gulf of California. *Geochim Cosmochim Acta* **58:** 5065–5082.

Solomon, E.A., Kastner, M., MacDonald, I.R., and Leifer, I. (2009) Considerable methane fluxes to the atmosphere from hydrocarbon seeps in the Gulf of Mexico. *Nat Geosci* **2:** 561–565.

Sommer, S., Pfannkuche, O., Linke, P., Luff, R., Greinert, J., Drews, M., *et al.* (2006) Efficiency of the benthic filter: biological control of the emission of dissolved methnae from sediments containing shallow gas hydrates at Hydrate Ridge. *Global Biogeochem Cycles* **20:** 14.

Tagliabue, A., Bopp, L., Dutay, J.-C., Bowie, A.R., Chever, F., Jean-Baptiste, P., *et al.* (2010) Hydrothermal contribution to the oceanic dissolved iron inventory. *Nat Geosci* **3:** 252–256.

Torres, M., McManus, J., Hammond, D.E., de Angelis, M.A., Heeschen, K., Colbert, S., *et al.* (2002) Fluid and chemical fluxes in and out of sediments hosting methane hydrate deposits on Hydrate Ridge, OR I: hydrological Processes. *Earth Planet Sci Lett* **201:** 525–540.

Treude, T., Krüger, M., Boetius, A., and Jorgensen, B.B. (2005) Environmental control on anaerobic oxidation of methane in the gassy sediments of Eckernförde Bay (German Baltic). *Limnol Oceanogr* **50:** 1771–1786.

Valentine, D.L. (2011) Fates of methane in the ocean. *Ann Rev Mar Sci* **3:** 147–171.

Walter, K.M., Zimov, S., Chanton, J.P., Verbyla, D., and Chapin, F., III (2006) Methane bubbling from Siberian thaw lakes as a positive feedback to climate warming. *Nature* **443:** 71–75.

Wankel, S.D., Germanovich, L.N., Lilley, M.D., Genc, G., DiPerna, C.J., Bradley, A.S., *et al.* (2011) Influence of subsurface biosphere on geochemical fluxes from diffuse hydrothermal fluids. *Nat Geosci* **4:** 461–468.

Webster, G., Newberry, C.J., Fry, J.C., and Weightman, A.J. (2003) Assessment of bacterial community structure in the deep sub-seafloor biosphere by 16S rDNA-based techniques: a cautionary tale. *J Microbiol Methods* **55:** 155–164.

Wegener, G., Shovitri, M., Knittel, K., Niemann, H., Hovland, M., and Boetius, A. (2008) Biogeochemical processes and microbial diversity of the Gullfaks and Tommeliten methane seeps (Northern North Sea). *Biogeosciences* **5:** 1127–1144.

Wellsbury, P., Mather, I., and Parkes, R.J. (2002) Geomicrobiology of deep, low organic carbon sediments in the Woodlark Basin, Pacific Ocean. *FEMS Microbiol Ecol* **42:** 59–70.

Wheat, C.G., McManus, J., Mottl, M.J., and Giambalvo, E. (2003) Oceanic phosphorus imbalance: magnitude of the mid-ocean ridge flank hydrothermal sink. *Geophys Res Lett* **30:** 1895.

## Supporting information

Additional Supporting Information may be found in the online version of this article:

**Fig. S1.** Fluorescent *in situ* hybridization (FISH) images of ANME-1 archaea and *Desulfosarcina-Desulfococcus* sulfate reducing bacteria from three different sediment temperatures (20°C, 55°C and 90°C). Probe specificity and hybridization conditions are described in Girguis and colleagues (2005) and the supporting information.

**Fig. S2.** Maximum-likelihood phylogenetic tree illustrating the relationships of 16 ssu rRNA ANME-1 sequences recovered from Middle Valley sediments to archaeal sequences from NCBI non-redundant database. Phylogenetic tree was generated with FastTree 2.0.0 (Price *et al.*, 2010) using minimum-evolution subtree-pruning-regrafting and maximum-likelihood nearest-neighbour interchanges. Local support values shown are based on the Shimodaira-Hasegawa (SH) test. The tree was rooted to *Pyrodictium occultum* (M21087). Scale = 0.09 substitutions per site.

**Fig. S3.** Fe K-edge XANES (left) and EXAFS (right) spectra for Middle Valley sediments. As revealed by a shift in the inflection point of the absorption edge to higher energies, XANES spectra reveal a dominance of Fe(II) in the upper sediments (0–3 cm) and mixed Fe(II)/Fe(III) in deeper sediments (below 6 cm). Spectra for the depths 0–3 and 3–6 cm, 6–9 and 9–12 cm, and 12–15 and 15–20 cm were nearly identical – one representative spectrum is shown for each interval. Standard spectra for iron sulfide (FeS) and lepidocrocite (γ-FeOOH) are included to illustrate the binding energies for Fe(II) and Fe(III) respectively. The Fe EXAFS spectra of sediments collected at 6–9 cm (black solid line) can be fit with a linear combination of standard spectra composed of green rust sulfate (32 mole %), siderite (24 mole %), and various Fe sulfides, including pyrrhotite, pyrite and mackinawite (44 mole %) ($\chi^2_{red} = 1.9$; R-factor = 0.06).

**Table S1.** Total cell densities in sediments incubated on the thermal gradient, continuous flow bioreactor (cells ml sediment$^{-1}$). Cells counts were obtained by filtering sediment cell suspensions, staining with SYBR I and counting at 100X on an epifluorescent scope with a gridded ocular.